# Manipulating Oxalate Decarboxylase Provides the Basis of Antilithic Therapy by Acting on the Gut Microbiota

Fang Wu[a], Yuanyuan Cheng[a#], Jianfu Zhou[b,c#], Peisen Ye[c#], Xuehua Liu[b], Lin Zhang[a], Rongwu Lin[c], Songtao Xiang[b *], Zhongqiu Liu[a*], Caiyan Wang[a*]

[a] International Institute for Translational Chinese Medicine, Guangzhou University of Chinese Medicine, Guangzhou, Guangdong, China

[b] Department of Urology, The Second Affiliated Hospital of Guangzhou University of Chinese Medicine, Guangzhou, China.

[c] The Second Clinical College, Guangzhou University of Chinese Medicine, Guangzhou, China.

Running Head: Oxalate Decarboxylase and $Zn^{2+}$ Acting on the Gut Microbiota - the Basis of Antilithic Therapy

*Address correspondence to S. Xiang, tonyxst@163.com.

*Address correspondence to Z. Liu, liuzq@gzucm.edu.cn.

*Address correspondence to C. Wang, wangcaiyan@gzucm.edu.cn.

Fang Wu, Yuanyuan Cheng, Jianfu Zhou and Peisen Ye contributed equally. Author order was determined on the basis of seniority.

## ABSTRACT

A high concentration of oxalate is associated with an increased risk of kidney calcium oxalate (CaOx) stones, and the degradation of exogenous oxalate mainly depends on oxalate-degrading enzymes from the intestinal microbiome. We found that Zinc Gluconate supplement to patients with CaOx kidney stones could significantly improve the abundance of oxalate metabolizing bacteria in human body through clinical experiments on the premise of simultaneous antibiotic treatment and the imbalance of *Lactobacillus* and OxDC was involved in CaOx kidney stones through clinical sample analysis. Then, we identified that $Zn^{2+}$ could be used as an external factor to improve the activity of OxDC and protect *Lactobacillus*, achieved the preventive effect on rats with stones aggravated by antibiotics. Finally, by analyzing the three-dimensional structure of OxDC and some *in vitro* experiments, we propose a hypothesis $Zn^{2+}$ increases the metabolism of oxalate in humans through its positive effects on *Lactobacillus* and OxDC to reduce CaOx kidney stone symptoms in rats.

## IMPORTANCE

Urinary stone disease is one of the most common urological disorders, and 70%-80% of urinary stones are calcium oxalate (CaOx) stones. We found the structural basis and metabolic mechanism by which oxalate decarboxylase metabolizes oxalate were elucidated, and $Zn^{2+}$ was illustrated to have therapeutic effects on CaOx stones by improving the tolerance of Lactobacillus to antibiotics. According to that, proper $Zn^{2+}$ levels in the diet, the consumption of more probiotic food and avoidance of the antibiotic overuse might be desirable measures for the prevention and treatment of

46 kidney stones.

47 **KEYWORDS:** CaOx stones, *Lactobacillus*, OxDC, $Zn^{2+}$

48

## Graphical Abstract

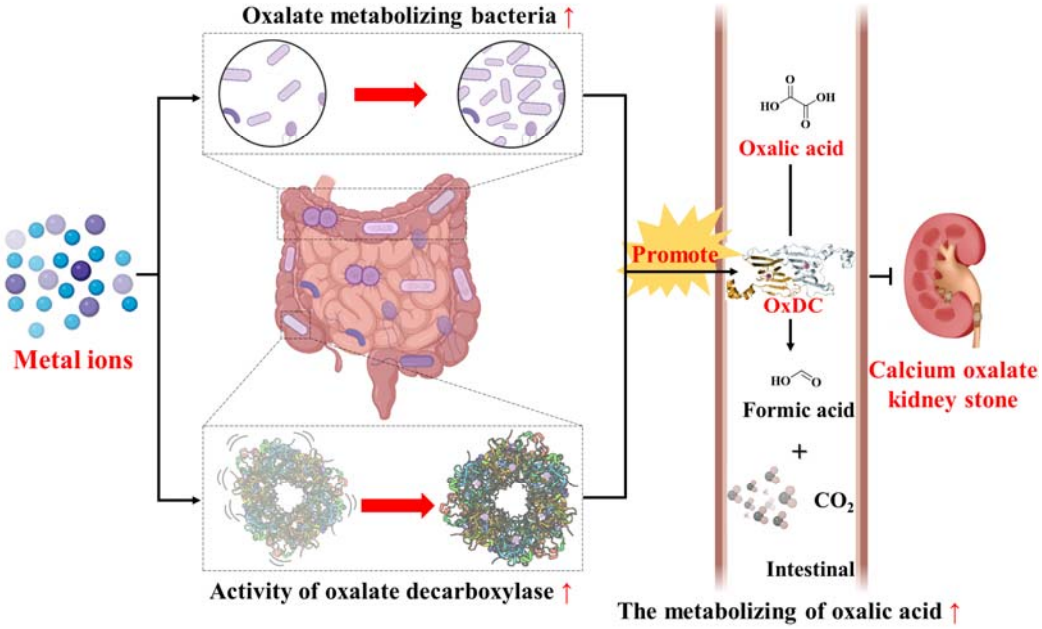

## Introduction

Urinary stone disease is one of the most common urological disorders (1), and 70%-80% of urinary stones are calcium oxalate (CaOx) stones (2-5). Clinically, patients with CaOx stones often exhibit hyperoxaluria and hypercalciuria (6); when oxalate excretion exceeds 40-45 mg per 24 h, the patient will be diagnosed with high oxaluria and is at risk for CaOx stones (7). The curved distal renal tubules exposed to a high concentration of oxalate over a long time are liable to form small crystalline nuclei that damage kidney epithelial cells and promote the formation of initial plaques. Eventually, plaques detach from the lumen, form a large CaOx stone and cause inflammation in the kidney (8, 9). Thus, the high content of oxalate in the human body is a major causal driver to kidney stones.

The human body does not contain any enzyme system for oxalate metabolism (10). Approximately 80% of exogenous oxalate is metabolized depending on oxalate-degrading bacteria (11, 12). Thus, the oxalate level in the kidneys is mainly modulated by the intestinal flora responsible for metabolizing oxalate. Moreover, long-term use or abuse of antibiotics causes intestinal flora disorder. In particular, the reduction of oxalate-metabolizing bacteria would significantly increase the risk of forming CaOx stones (13, 14). Accordingly, maintaining the balance of the intestinal flora in the human body and increasing the number of oxalate-degrading bacteria positively effect on patients with CaOx stones.

At present, although the treatment of kidney stones has evolved to advanced minimally invasive surgery, the recurrence rate of stones is still in a high level (15, 16). Therefore, it is important to discover new effective treatment strategies for CaOx stones patients. *Lactobacillus* strains are commonly used in dairy products and medical probiotic formulations due to their efficiency and safety (17-20). Recently,

Campieri *et al* (21-25) have found that the oxalate content and stone size were significantly reduced in patients with hyperoxaluria after the *Lactobacillus's* administration. The degradation of oxalate by *Lactobacillus* is attributed to the expression of oxalate decarboxylase (OxDC) (26). The therapeutic effect of OxDC was further confirmed by the CaOx stones rat models (27). Besides, *Lactobacillus* can strengthen the intestinal barrier by regulating the expression of tight junction protein and the body's immune response (28, 29), playing an important role in maintaining the balance of intestinal flora (30). Given the advantages of *Lactobacillus* and OxDC mentioned above, it has become a promising and potential strategy for the treatment of CaOx stones patients. Nevertheless, the oxalate's metabolic mechanism by OxDC is still largely unknown, limiting the widespread use of *Lactobacillus* and OxDC in the clinic.

Zinc is the second most abundant essential trace element that plays a vital role in maintaining the normal function of the human body (31). Zinc serves as a metal cofactor for more than 300 enzymes (32), and has an anti-inflammatory function (33). As probiotics, *Lactobacillus* has a good zinc enrichment effect, which increases their antibacterial activity in the intestine (34). If zinc can improve the ability of *Lactobacillus* to degrade oxalate in the intestine or enhance its viability, it would play a positive role with the treatment of CaOx stones.

In this study, we learned that in clinical treatment experience supplementation of Zinc Gluconate for CaOx kidney stone patients would improve the gut microflora diversity and the abundance of of *Lactobacillus*. Thus, we explored the relationship among the $Zn^{2+}$, *Lactobacillus* and oxalate metabolism. Firstly ,The protective effect of $Zn^{2+}$ on *Lactobacillus* was discovered *in vitro*, and it was further confirmed that $Zn^{2+}$ had a relieving effect on CaOx kidney stone symptoms aggravated by antibiotics

*in vivo*. Secondly, it was found that the content of OxDC in patients with CaOx kidney stones was abnormal significantly, suggesting that there may be abnormal oxalate metabolism in patients, and then based on the co-crystal structure of OxDC and formic acid, combined with enzyme activity and cell assays, we elucidated the mechanism of oxalate degradation by OxDC. Finally, we found that $Zn^{2+}$ could improve the stability and oxalate-degradation activity of OxDC and determined its specificity for OxDC and *Lactobacillus*. In a word, we demonstrated that $Zn^{2+}$ supplementation may alleviate symptoms in patients with CaOx kidney stones by increasing the enzymatic activity of OXDC as well as the abundance of *Lactobacillus*.

## Results

### Supplementation of Zinc Gluconate on gut microflora for patients with CaOx kidney stones

The excessive intake of oxalate and its metabolic disorders are key triggers of CaOx kidney stones formation. The oxalate metabolism is mainly dependent on four types of intestinal bacteria in human, including *Oxalobacter, Lactobacillus, Enterobacteriaceae,* and *Bifidobacterium*. In clinical treatment, we found feces in patients with CaOx kidney stones was improved after Zinc Gluconate therapeutics. We recruited 40 subjects and divided them into four cohorts, i.e.: non-kidney stones group (n=10), CaOx kidney stones group (n=10), CaOx kidney stones treated with antibiotic group (n=10), and CaOx kidney stones treated with antibiotic and Zinc Gluconate group (n=10). The feces of subjects were used as samples to determine the abundance of several important intestinal flora in human intestinal (**Figure 1A**). Analysis of intestinal microbes showed that the abundance of *Bacteroidota* and *Actinobacteriota* changed significantly. However, the change of human beneficial bacteria *Firmicutes* was not obvious in four groups (**Figure**

**1B**). Therefore, we further investigated *Lactobacillus* in *Firmicutes,* it was found that the abundance of *Lactobacillus* decreased significantly in the CaOx kidney stones group but increased significantly after Zinc Gluconate supplementation. At the same time, we also measured the abundance of two other oxalate metabolizing bacteria in human intestine, which was similar to the trend of *Lactobacillus* (**Figure 1C**). These results showed that administration of Zinc Gluconate supplement to patients with CaOx kidney stones could significantly improve the abundance of oxalate metabolizing bacteria in human body, especially with the premise of simultaneous antibiotic treatment. Similarly, we also detected changes in the diversity of intestinal flora, and the types of intestinal flora in patients with kidney stones were significantly reduced. After antibiotic-based treatment, the species of bacteria continued to decline, but after the adjuvant treatment with Zinc Gluconate, the number of species of bacteria almost returned to a normal level (**Figure 1D**).

**The protection of $Zn^{2+}$ on *Lactobacillus* and the therapeutic effect on rats with CaOx stones**

According to clinical investigation, the abuse of antibiotics can lead to an imbalance of the human intestinal flora, so it is often regarded as a potential kidney stones trigger (35). *L. casei* is a kind of probiotics belonging to the genus *Lactobacillus* commonly used in life. Therefore, to screen out which antibiotic is extremely sensitive to *L. casei*, we used seven common antibiotics to interfere with the survival of *L. casei* (**Figure 2A**) and found that *L. casei* had the strongest sensitivity to ampicillin (Amp), chloramphenicol, and penicillin. Finally, we chose Amp as an inhibitor of *Lactobacillus* in subsequent assays. Then we tested the effect of different metal ions on intestinal flora. As expected, we found that $Zn^{2+}$ could

promote the growth of flora (**Figure 2B**). With the treatment with Amp, $Zn^{2+}$ addition was significantly increased the survival rate of *L. casei* compared with other common divalent metal ions (**Figure 2C**). Since excessive oxalic acid inhibits the growth of *Lactobacillus*, we subsequently investigated the effect of $Zn^{2+}$ on the tolerance of *Lactobacillus* and *L. casei* towards oxalic acid by adding $Zn^{2+}$ to DeMan Rogosa-Sharpe (MRS) medium with the supplement of oxalic acid. The impact of $Zn^{2+}$ on the survival of *Lactobacillus* and *L. casei* under the Amp condition was also investigated similarly. The addition of $Zn^{2+}$ increased the tolerance of *L. casei* to oxalic acid (**Figure 2D**). The assay results also showed that $Zn^{2+}$ could hold back the inhibition effect of oxalic acid or Amp on *L. casei*. The addition of $Zn^{2+}$ could promote proliferation and increase survival rate of *L. casei*. According to literature reports, $Zn^{2+}$ reusation of increased *E.coli* by relieving oxidative stress, and further promote the transcription of AdcA and AdCB by regulating the transcription inhibitor AdcR, thereby promoting the gene transcription translation of Streptococcus and increasing bacterial proliferation (36,37). These results indicated that $Zn^{2+}$ may achieve protective effect by regulating the oxidative stress and transcriptional translation process of *L. casei* (**Figure 2E**).

**The effect of $Zn^{2+}$ on the inflammatory response and the degree of kidney damage**

We further intent to explore whether $Zn^{2+}$ had a certain effect on CaOx stones *in vivo*. Based on the H&E staining results, the rats with stones aggravated by antibiotics had a larger CaOx stone area compared to the control group. However, after the addition of $Zn^{2+}$, the stone area reduced significantly compared to antibiotics aggravated stones rats (**Figure 3A**). To better evaluate the degree of damage of kidney stones in rats, we used osteopontin (OPN) as an indicator. OPN

is one of the main organic components of CaOx stone matrix. The abnormal high content of OPN could accelerate the release of adhesion factors, increase kidney damage, and promote kidney inflammation (36)(**Figure 3B**). To further verify the therapeutic effect of $Zn^{2+}$ on rat models with stones exacerbated by antibiotics, we measured inflammation-related indicators. We found that OPN and CD44 mRNA levels in the kidney of the stone group and the "Amp+Stone" group were significantly increased compared with the control group (**Figure 3C**). Secondly, urea nitrogen in serum increased significantly, while urea nitrogen excreted in the urine reduced remarkably in the "Amp+Stone" group, which indicated that the kidney was damaged, but given zinc supplements group did not change significantly (**Figure 3D**). Finally, we also tested the expression level of inflammatory factors (TNFα, IL-1β) and zinc supplements administration suppressed the mRNA level of TNFα and IL-1β (**Figure 3E**). These results further illustrated that $Zn^{2+}$ had a certain therapeutic effect on rats with stones exacerbated by antibiotics.

**Imbalance of OxDC in CaOx kidney stones patients and the overall structure of *L. farciminis* OxDC**

Previously, we demonstrated that $Zn^{2+}$ could promote the abundance of beneficial intestinal microflora and CaOx metabolism. Since *Lactobacillus* was reported to express OxDC to degrade oxalate (26), which had great potential for the treatment of CaOx stones, we further evaluated the mRNA level of OxDC in two groups. Compared with that in the non-kidney stones patients' group, the mRNA level of OxDC reduced sharply in the CaOx kidney stones patients' group (**Figure 4A**), consistent with the low level of *Lactobacillus* in the CaOx kidney stones patients. These results implied that both OxDC and *Lactobacillus*'s concentration might be

closely related to the formation of CaOx stones.

Considering the importance of *L. farciminis* OxDC in the degradation of CaOx kidney stones, we intended to explore the metabolic mechanism of OxDC started from protein structure. We constructed the expression system of OxDC *in vitro*, and the chromatographic peak of OxDC showed a single symmetrical peak at the elution position between markers 440 kDa and 158 kDa (**Figure 4B**). The OxDC gene of *L. farciminis* encodes 410 amino acids (aa), which contains a N-terminal cupin domain (aa 56-233) and C-terminal cupin domain (aa 234-373). Fortunately, our crystal structure captures the active state of OxDC, which contains one metabolite formic acid in the N-terminal cupin domain (**Figure 4C left**). However, no electron density for formic acid was observed in the C-terminal cupin domain (**Figure 4C right**), The topological structure of the two domains is similar, with each consists of 11 β-sheets (**Figure 4D**). The RMSD value is 0.189 Å between the cupin domains, superimposition of both domains revealed no noticeable backbone movement or meaningful shift of the ligand position (**Figure 4E**). This phenomenon was highly likely due to the method of preparation of the crystal of the enzyme-substrate complex. The crystal structure of OxDC in complex with formic acid was resolved to a resolution of 2.79 Å by molecular replacement (**Table 1**). The structure of OxDC belongs to space group $P_{21}$, with each asymmetric unit containing six OxDC molecules. This assembly state in crystal structure agreed with the chromatographic peak of OxDC. The overall structure of OxDC retains the conserved fold and sandwich morphology of the cupin family. In terms of internal interactions, the N-terminal of the upper layer of monomers were attached to the C-terminal of the lower layer and in the same layer, each pair of adjacent subunits were also joined by an interaction between the N-terminal and C-terminal domain, forming a stable

triangular-like spatial conformation. A hollow cylindrical intermediate structure could be observed by structure rotating 90° along the Y-axis (**Figure 4F**). Metal ion was dispensable for cupin family proteins to carry out diverse biological functions (37), in OxDC structure, there were twelve endogenous $Mn^{2+}$ evenly distributed in the two domains of each subunit, which were crucial for metabolizing the oxalate.

**Key residues for oxalate degradation by OxDC**

OxDC degrades oxalic acid to formic acid and carbon dioxide. Based on analysis of conservation of the OxDC protein sequence and the structure of the protein in complex with formic acid, we found that each of the $Mn^{2+}$ binding sites was coordinated by two highly conserved glutamate residues and three histidine residues in the cupin fold (**Figures 5A-C**). In the active conformation of OxDC, the formic acid molecule near $Mn^{2+}$ interacted with the E162 in the N-terminal cupin domain, which was consistent with the previously reported state of *B. subtilis* OxDC (38).

We selected five conserved residues (H95, E162, H275, E333, and Y340) from the N and C-terminal cupin domains to investigate their role for the oxalate-degradation activity of OxDC by using oxalic acid as substrate with the methylene blue-potassium dichromate system. Compared with the wild type (WT) OxDC, the activity of mutants (H95Q, E162D, H275Q, and E333D) all severely harmed, confirming the crucial role of these four residues (**Figure 5D**). Mutant Y340N was equally active as WT OxDC. It was likely that the Y340 residue did not participate in the catalytic activity of oxalic acid, and it was not structural conservation among these five residues. Notably, according to previous literature reports (39), the N-cupin domain was a key site for catalytic activity. Here, we found

that the residues H275 and E333 in the C-cupin domain also had a significant influence on enzyme activity. Overall, both the C-cupin domain and N-cupin domain have a certain coordination effect on the catalytic process of OxDC.

To further verify the important role of the two residues (E162 and E333) interacting with $Mn^{2+}$ in the two domains, respectively, we evaluated the metabolism of oxalate for WT OxDC and these two mutants at the cellular level. When OxDC was transfected into cells, exogenous OxDC could metabolize oxalic acid after being expressed by cells, reducing the toxic side effects of oxalic acid on HEK293 cells. We created a cytotoxic oxalate cellular environment, the successful transcription of exogenous genes was detected by the experimental methods of qRT-PCR and fluorescence microscope photographing (**Figure 5E**), and then found that the mRNA levels of apoptosis factor (Caspase3) and cellular inflammatory factors (IL-1β, TNFα) in $HEK293^{E162D}$ and $HEK293^{E333D}$ cells were higher than those in $HEK293^{WT\ OxDC}$ cells (**Figure 5F**). This finding indicates that mutation of E162D and E333D could impair the oxalate-metabolization activity of OxDC.

**Discovered and verified the special effect of $Zn^{2+}$ on OxDC**

During the catalytic process, oxalate and dioxides bind $Mn^{2+}$ to form a formyl radical anion intermediate to facilitate OxDC to metabolize oxalate to formate and $CO_2$, thereby completing the decarboxylation reaction (40). Since OxDC is a metal-dependent enzyme, we explored the effects of common divalent metal ions on protein activity. The activity of OxDC in supplied with $Ca^{2+}$, $Mg^{2+}$, and $Sr^{2+}$ were almost as same as the control group, indicating no effect on the activity of OxDC.

While the addition of $Zn^{2+}$ and $Mn^{2+}$ to OxDC retain the protein activity equally (**Figure 6A**). Given the good effect of $Zn^{2+}$ on healthy intestinal flora, we emphatically analyzed $Zn^{2+}$ for OxDC. The circular dichroism (CD) result revealed that $Zn^{2+}$ generated similar effect on the secondary structure of the protein as $Mn^{2+}$ did. Among them, α-helices decreased, while the proportion of β-sheets and β-turns was increased (**Figure 6B**), indicated that OxDC has the binding force to metal ions $Mn^{2+}$ and $Zn^{2+}$. Besides, $Zn^{2+}$ improved the stability of the protein significantly (**Figure 6C**). ITC assay result showed that the binding capacity of $Zn^{2+}$ to the EDTA treated OxDC was 130 times that of the untreated group, indicating that $Zn^{2+}$ was likely to improve the thermostability and activity through competing with `$Mn^{2+}$ to bind the active pocket of OxDC (**Figures 6D-E**).

**The effect of $Zn^{2+}$ on the digestive stability of OxDC *in vitro***

Previous studies have shown that the metal ion was important of OxDC activity, the supplementation of $Zn^{2+}$ can increase OxDC's activity and $Mn^{2+}$ evenly distributed in the two domains of OxDC, which are crucial for metabolizing the oxalate. The result of chromatogram from size-exclusion chromatography analysis showed that OxDC exists in two major forms which are dimer and hexamer the functional aggregation state and 1mM EDTA reduce the hexamer of OxDC, because EDTA can attract metal ions likes $Zn^{2+}$ and $Mn^{2+}$ and induce the stability and activity of OxDC. When supplementing superfluous $Zn^{2+}$ and $Mn^{2+}$, the hexamer of OxDC can recover (**Figure 7A**). The same as OxDC protein thermal shift assay, add $Zn^{2+}$ and $Mn^{2+}$ can resist the reduce of $\Delta T_m$ from EDTA (**Figure 7B**). In addition, following previous

294 experiment we detected the digestive stability of OxDC with trypsin *in vitro*. As
295 displayed in **Figure 7C**, the signal of the OxDC band (~44 kDa) decreased slowly as
296 digestion time increased, indicating that the degradation of OxDC by trypsin was
297 slight after 10 min and serious more than 30min. When the metal ions like $Zn^{2+}$ and
298 $Mn^{2+}$ was superfluous, the major band of OxDC was recovered. In summary, metal
299 ions were important for OxDC especially $Mn^{2+}$ mentioned earlier. Our study found
300 that $Mn^{2+}$ can maintain the activity and structures stability. The activity of OxDC will
301 be destroy, when $Mn^{2+}$ attracted by EDTA. Adding superfluous $Zn^{2+}$ can rebuild its
302 activity and structures stability which improve the metabolism of Oxalic acid (**Figure**
303 **7D**).

304 **Discussion**

305 In recent years, the relationship between oxalate-degrading bacteria and CaOx
306 stones becomes research hot spots. In this study, we designed clinical trials and
307 analyzed many clinical samples to further confirm that the *Lactobacillus* is closely
308 related to the occurrence of CaOx stone and first found that the zine gluconate can
309 increase the abundance of oxalate metabolizing bacteria in the intestine of CaOx stone
310 patients. This finding shows that a reduction in the number of *Lactobacillus* may lead
311 to a decline in the OxDC content, thereby reducing the metabolism of oxalate by the
312 intestinal flora and increasing the incidence of CaOx stones, and supplementing zine
313 gluconate has a positive effect on oxalate metabolizing bacteria.

314 Interestingly, we found that when conserved residues that interact with $Mn^{2+}$ in
315 the C-terminal cupin domain were mutated, the activity of the enzyme was also
316 significantly decreased. This indicates that both metal sites are important and show
317 synergy in the metabolism of oxalate. In addition, weak metabolic activity was still

observed after key residues were mutated. This is related to the fact that OxDC can be converted into an oxalate oxidase under certain conditions. Because OxDC is likely to have evolved from oxalate oxidase by gene replication and exhibits strong sequence conservation with oxalate oxidase (41), however, the products of OxDC and oxalate oxidase are different, for example, oxalate oxidase can metabolize oxalate into hydrogen peroxide and carbon dioxide (42).

During the experiment, we found that $Zn^{2+}$ has a protective effect on *Lactobacillus* under an antibiotic environment. According to reports, $Zn^{2+}$ can be enriched by *Lactobacillus* by binding to peptidoglycan in the bacterial cell wall (21). Simultaneously, antibiotics mainly destroy the cell wall structure of bacteria, causing the cells to burst and die. We preliminarily believe that when $Zn^{2+}$ is present around the *Lactobacillus*, $Zn^{2+}$ will combine with the hydroxyl group, carboxyl group, and the other anions in the peptidoglycan structure of the bacterial cell wall to increase the density of the cell wall structure. Thereby *Lactobacillus* is immune to the interference of antibiotics, which might contribute to the protective effect of $Zn^{2+}$ to *Lactobacillus*.

OxDC is an $Mn^{2+}$-dependent enzyme, and $Mn^{2+}$ acts as a ligand for the redox cycle in the process of oxalate metabolism. $Zn^{2+}$ and $Mn^{2+}$ are two common divalent ions. We firstly found that $Zn^{2+}$ can competitively bind to the $Mn^{2+}$ binding pocket in OxDC, when all the metal ions contained in the protein itself were chelated by EDTA, the binding capacity of OxDC to $Zn^{2+}$ was increased by about 100 times. This shows that $Zn^{2+}$ can not only occupy the 12 binding sites of $Mn^{2+}$ but may also occupy the binding sites of other metal ions, and it can increase the protein stability and change the secondary structure to enhance OxDC's ability to bind and metabolize OA. At present, the precise relationship between $Zn^{2+}$ and kidney stones is unknown. The earliest studies showed that the amount of urinary $Zn^{2+}$ excreted from patients with

343 stones mostly differs from that of healthy people (43), but this study was greatly
344 affected by sex-related difference and individual difference. In a recent literature
345 report, $Mg^{2+}$ improved the survival rate of *B. subtilis* by regulating antibiotics that
346 target the ribosome. We speculate that $Zn^{2+}$ has a similar function. Therefore, we
347 designed clinical trials and found that zine gluconate can indeed increase the
348 allowance of *Lactobacillus* in the intestine of CaOx stone patients. However, the
349 overall effect of zine gluconate on *Firmicutes* has little change. It is possible that zine
350 gluconate not only increases the content of oxalate metabolizing bacteria, but also
351 inhibits the abundance of some intestinal flora in *Firmicutes*, which needs to be
352 further researched. In this paper, we explored the specific effect of $Zn^{2+}$ on kidney
353 stones from the perspective of *Lactobacillus* in the intestinal flora and OxDC
354 originating from *Lactobacillus* for the first time, and our results provide a new
355 strategy and direction for the prevention in stones via metal ions.

356 In recent years, among the four oxalate degrading bacteria, researchers have
357 focused more on the relationship between CaOx stones and *Oxalobacter*. However,
358 *Oxalobacter* is very sensitive to antibiotics and is present in the intestines of only
359 60%-80% of adults. Bariatric surgery, bowel disease, and cystic fibrosis all inhibit the
360 recolonization of *Oxalobacter* in the intestine (44). In addition to its stability and high
361 safety, *Lactobacillus* also has the strength of the intestinal barrier, body's immune
362 response, and play an important role in maintaining the balance of intestinal flora.
363 These characteristics of *Lactobacillus* provide a theoretical basis for the development
364 of related preparations to treat CaOx stones in the future.

365 Here, the structural basis and metabolic mechanism by which
366 oxalate decarboxylase metabolizes oxalate were elucidated, and $Zn^{2+}$ was illustrated
367 to have therapeutic effects on CaOx stones by improving the tolerance of

368 *Lactobacillus* to antibiotics. According to our research, proper $Zn^{2+}$ levels in the diet,
369 the consumption of more probiotic food and avoidance of the antibiotic overuse might
370 be desirable measures for the prevention and treatment of kidney stones.

371 **Methods**

372 **Materials and reagents**

373 The OxDC gene derived from *L. farciminis* (GenBank accession number:
374 CP012177.1) was constructed by GenScript company (Nanjing, Jiangsu, China) and
375 cloned into the pET-20b (-) vector. *E. coli* DH5α and BL21 (DE3) were the host
376 strains for plasmid amplification and protein expression, respectively. The *Nde*I and
377 *Xho*I restriction enzymes were purchased from Thermo scientific. Ni-NTA column,
378 HisTrap HP 1mL and Superdex 200 increase 10/300GL resin were all purchased from
379 GE Healthcare. SYPRO Orange protein gel staining 5000x and PrimeScriptTM RT
380 reagent Kit were purchased from Thermo Fisher Scientific. *L. casei* was a gift from
381 Macau University of Science and Technology. oxalic acid, sodium oxalate, $NH_4Cl$,
382 and EG were purchased from Sigma-Aldrich. Chloramphenicol, clindamycin,
383 vancomycin, ampicillin, kanamycin, penicillin, gentamicin was supplied by Ruishu
384 Bio. Zinc Gluconate was purchased from the hospital. Other chemicals used were
385 biochemical research grade. *L. casei* was selected for all *Lactobacillus* assays in this
386 study.

387 **Patients and samples**

388 This research was approved by the Human Ethics Committee of Guangdong
389 Provincial Hospital of Chinese Medicine (Guangzhou, Guangdong, China). An

informed consent form was signed by all patients in the study (ZF2020-059-01). The clinical data and samples were harvested from the Second Affiliated Hospital of the Guangzhou University of Chinese Medicine (Guangzhou, Guangdong, China) from July 2018 to January 2022. The inclusion criteria for patients in figure 1 were as follows: 1) diagnosis of CaOx kidney stones, 2) age of 20-60 years, 3) glomerular filtration rate below 60 ml/min/1.73 $m^2$, 4) no uptake of drugs or food to regulate the intestine within the past one month, and 5) no significant changes in diet. The exclusion criteria were as follows: 1) stones with the tumor or bladder stones, 2) hypotension, hypernatremia, or a history of congestive heart failure, 3) pregnancy, 4) hyperthyroidism, adrenal diseases, pituitary tumors, or other diseases that affect calcium regulation, 5) present history of intestinal disease or history of major gastrointestinal surgery, 6) serious heart, brain, liver, kidney or other systemic diseases or mental illness, or 7) severe urinary tract infection. In Figure 1, we divided the subjects into antibiotic treatment group, the antibiotic combines with Zinc Gluconate group, the patients with CaOx Kidney stones group and the patients with No-kidney stones group. Each group contained ten subjects. Using 16SRNA technology to measure the stool of patients, and the subjects had good compliance. The CaOx composition of the stones was confirmed by infrared spectrum analysis. Feces were provided as a specimen of all participants.

**The influence of external factors on the growth of *L. casei***

MRS medium was subjected to high-temperature steam sterilization and used as the culture medium for *L. casei*, a strain of *Lactobacillus*. Through drug sensitivity

412 assays, we examined the effects of seven antibiotics (chloramphenicol, kanamycin,
413 ampicillin, vancomycin, clindamycin, penicillin, and gentamycin) on *L. casei* growth.
414 *L. casei* was cultured in MRS medium containing antibiotic at a final concentration of
415 0.1 μg/ml. To explore the effect of $Zn^{2+}$ on the oxalic acid tolerance of *L. casei*, oxalic
416 acid was added at a three-concentration gradient (1, 5, and 10 mM) and 2 mM $Zn^{2+}$ to
417 the MRS medium used to culture *L. casei*. To test the effects of $Zn^{2+}$ supplementation
418 on the antibiotic tolerance of *L. casei*, 0.8 μg/ml antibiotic and $Zn^{2+}$ at 2 mM and 10
419 mM were used. The absorbance was measured at $OD_{600}$ with a microplate reader at
420 fixed time points. This method was based on previously reported literature (45).

421 **Animal experiments**

422 Six-week-old male Sprague-Dawley (SD) rats were purchased from Southern
423 Medical University, and the animal protocol was approved by the Animal Care
424 Committee (SYXK2019-0144). The SD rats were housed at 22 ± 2 °C in standard
425 cages in a specific pathogen-free facility under a 12-h and 12-h light-dark cycle.
426 Water and chow were available ad libitum. After the weights of the SD rats were
427 measured, they were randomly divided into 5 groups containing 5 rats each. The rats
428 in control group received normal rat chow and drinking water. Rats in groups -
429 "Stone", "Amp+Stone", and "Amp+$Zn^{2+}$+Stone" were received food containing
430 0.4% $NH_4Cl$ and 1% EG from day 14 to day 29 to form CaOx kidney stones. Rats
431 in group- "Amp+$Zn^{2+}$+Stone" was received supplemental $Zn^{2+}$ for 29 d, while rats
432 in group- "Amp+Stone" and "Amp+$Zn^{2+}$+Stone" were received antibiotics for 29
433 d. Amp and $ZnSO_4$ were dissolved in ultrapure water and administered by gavage

to the rats every day at 9:00 and 16:00 at doses of 20 mg/kg and 10 mg/kg (body weight). Kidney, urine, and blood were collected on days 3, 5, 7, 9, 11, 13, and 15 during the experiment. The body weight of the animals was monitored, and a urine sample (24 h) was used to detect pH. The kidney was subjected to H&E staining to observe the growth of the stone, and the collected serum was used to measure the $Zn^{2+}$ content. All the animal experiments involved in this study were approved by the Institutional Animal Care and Use Committee of the Guangzhou University of Chinese Medicine.

We choose the EG to build a CaOx kidney stones model, and this method consists of the administration of 0.4% $NH_4Cl$ and 1% EG, the precursor of oxalic acid, which increases the concentration of uric acid, while $NH_4Cl$ acidifies the urine and accelerate the growth of stones (46). $NH_4Cl$ and EG dissolved in ultrapure water to final concentrations of 0.4% and 1%, respectively, were administered in the drinking water, which was freely available to the rats for 15 d. The rats were dissected and assessed for kidney stones growth on the $14^{th}$, $17^{th}$, $19^{th}$, $21^{st}$, $23^{rd}$, $26^{th}$, and $29^{th}$.

**Hematoxylin-eosin staining**

After the kidney tissues were washed with 0.9% normal saline, they were first fixed with 4% paraformaldehyde for 48 h and then dehydrated, waxed, and paraffin sectioned to a thickness of 4 μm. The sections were further dewaxed with xylene and eluted with a gradient of ethanol. Finally, the sections were dehydrated, permeabilized and sealed by dying with Yin Hong staining for 2 min, and finally dehydrated with ethanol, then permeabilized and sealed, completing the HE stains process. Prepared

tissue sections were observed under an optical microscope at a 200× magnification.

**Determination of urea nitrogen in serum and urine**

Centrifuge the collected rat blood samples at 4°C, 3000 rpm for 10 min, and collect the supernatant. Dilute the collected serum samples by 5 times, and then use the urea nitrogen detection kit for content determination. Urea is hydrolyzed under the action of adenase to produce $NH_4^+$ and $CO_2$. $NH_4^+$ generates blue substance with phenol developer in alkaline environment. The amount of blue substance produced is proportional to the content of urea nitrogen, which is used as a calculation. Similarly, the collected rat urine was diluted 5 times and tested in the same way. Finally, calculate according to the formula on the manual.

**Collection of stool samples, 16S RNA sequencing, and data analysis**

To detect the changes in the intestinal flora of the four groups of volunteers recruited, we collected volunteer feces on a regular basis. Professional collection was performed by nurses with the permission of volunteers. Finally, the collected samples were sent to Majorbio for determination.

**Construction of vectors**

We constructed a truncated protein consisting of the main body of *L. farciminis* OxDC (aa 22-373, WT) using recombinant cloning technology and obtained five mutant plasmids (H95Q, E162D, H275Q, E333D, and Y340N) using *QuikChange* technology. The truncated OxDC gene was subcloned into the pET-21b (-) vector with a C-terminal 6×His tag, and the WT and mutant genes were subcloned into the pET-20b (-) vector. PCR-amplified WT, E162D and E333D fragments were cloned

into the pEGFP vector at the *Nhe*I and *BamH*I restriction sites and expressed in the eukaryotic expression vector pEGFP. All recombinant plasmids were confirmed by PCR and DNA sequencing.

**Protein expression and purification**

The proteins were overexpressed in the *E. coli* BL21 (DE3) and Rosetta (DE3) strains. Bacterial cultures were grown in LB medium at 37 °C. When the $OD_{600}$ was 0.6-0.8, cells were induced with isopropyl β-D-1-thiogalactopyranoside to a working concentration of 0.2 mM. After incubation at 25 °C overnight, *E. coli* cells were centrifuged for 20 min at 4,000 rpm, and cell lysates were obtained with a cryogenic grinder and then centrifuged at 14,000 rpm for 1 h at 4 °C to obtain the supernatant. The resulting supernatant was roughly purified using Ni-NTA agarose resin (GE Healthcare, Sweden). Further purification method was carried out with a 1 mL HisTrap HP column (GE Healthcare, Sweden) to obtain the pure protein. Since crystals of the full-length protein do not diffract, the truncated protein corresponding to the body of OxDC (aa 22-373) was prepared for the crystallographic experiment. All proteins were purified in a similar manner.

**Size-exclusion chromatography analysis**

Using an AKTA pure 25 M1 (GE Healthcare, Sweden) purification system with Superdex 200 increase 10/300 GL resin column, the state of the protein in solution was examined. The target protein was centrifuged at 14,000 rpm for 10 min at 4 °C before loxalic acidding, and the eluted solution contained 20 mM Tris-HCl (pH 8.0), 150 mM NaCl, and 1 mM DTT. Three protein standards (440 kDa, 158 kDa, 75 kDa)

were dissolved together in the same solution as target protein and separated by gel filtration chromatography.

**Crystallization, data collection, and structure determination**

Purified OxDC was concentrated to approximately 3.5 mg/ml. The initial crystal was obtained using a commercial screening kit (Index) with the 96 well sitting-drop vapor diffusion method. In the optimization process, 2 mM $Mn^{2+}$ and 10 mM oxalate were incubated with the protein in an acidic environment for 1 h at 4 °C. The protein and the reservoir solution were mixed in a 2:1 volumetric ratio. The best crystals were produced in a reservoir solution containing 18% PEG3350, 0.2 M $NH_4Cl$, 0.2 M sodium dihydrogen phosphate, and 0.2 M Bis-Tris (pH 5.5). The selected crystals were soxalic acidked for 1-3 min in a protective solution containing all the components of the reservoir solution supplemented with 20% glycerol (v/v), and crystals were then immediately flash frozen in liquid nitrogen. Data collection was performed at beamline 17U (BL17U1) of the Shanghai Synchrotron Radiation Facility (SSRF, Shanghai, People's Republic of China), and data processing was carried out with the program HKL2000. Molecular replacement was performed with CCP4 software using the known structure of *B. subtilis* OxDC (PDB ID: 1UW8) as a search model. By further build model manually with Coot software (47), the structure of *L. farciminis* OxDC at a resolution of 2.79 Å was finally obtained.

**Cell culture and treatment**

HEK293 cells were purchased from China Center for Type Culture Collection (CCTCC) and cultured in Dulbecco's modified Eagle's medium (DMEM)

supplemented with 10% fetal bovine serum, 100 U/ml penicillin and 0.1 mg/ml streptomycin. The incubation conditions were 37 °C, 95% humidity and 5% $CO_2$. Transfection of cells at a specific stage of cell culture was performed according to the instructions of a transfection kit (Hanbio, China). After 24 h, transfectants with a fluorescence signal appeared. The overexpression of foreign genes was further confirmed by qRT-PCR.

Cell viability was evaluated by the MTT method. HEK293 cells expressing recombinant pEGFP, $pEGFP^{WT}$, $pEGFP^{E162D}$ and $pEGFP^{E333D}$ were treated with 0 μmol, 50 μmol, 250 μmol, 500 μmol, 750 μmol, or 1000 μmol of oxalate. After the cells were further cultured, MTT was added to the cell medium at a final concentration of 0.5 mg/ml and incubated for 4 h. The cell culture plate was removed from the incubator, 200 μl of DMSO was added to dissolve the crystal violet, and the absorbance was then immediately recorded at $OD_{570}$ after incubation on a shaker in the dark for 5 min. The optical density of each well was subtracted from blank control well. After analysis of the results, 750 μM oxalate was selected to generate a toxic oxalate environment.

**_In vitro_ enzyme activity assay**

The enzymatic activities of the WT and mutant OxDC proteins were examined by methylene blue-potassium dichromate assay. Pure proteins containing 5% glycerol were mixed with oxalic acid at a molar ratio of 1:100, and all enzymatic solutions were incubated in a reaction system of 100 mM NaCl and 40 mM Bis-Tris (pH 5.5) for 2 h at room temperature. The reaction was terminated by the addition of 600 μl of

1 M $H_2SO_4$. Then, the remaining concentration of oxalic acid in the enzyme reaction system was determined immediately by methylene blue-potassium dichromate redox catalysis. Finally, the absorbance of the reaction solution at $OD_{660}$ was measured, and a standard linear relationship was established between the oxalic acid concentration and the absorption value. All assay results were repeated five times or more.

**Protein thermal shift**

SYPRO Orange protein gel staining 5000× (Thermo scientific, USA) was diluted to 200x with 40 mM Bis-Tris (pH 5.5), 100 mM NaCl, and 1 mM DTT. All protein samples were concentrated to about 4 mg/ml. The assay contains two groups, one group was used to investigate the effect of adding $Zn^{2+}$ on OxDC, and the other group was used to explore the effect of adding $Zn^{2+}$ on OxDC after incubating with 2 mM oxalic acid. 2 mM $Zn^{2+}$ was incubated with the protein for 1 h, and then centrifuged it at 14000 rpm for 10 min for detection. The total 20 μl reaction system was mixed with 5 μl SYPRO Orange protein gel staining 200× and 20 μg protein. The sample was gradually heated from 25 to 90 °C at a gradient of 0.2 °C /min and analyzed by qRT- PCR instrument. All protein thermal shift figures were produced by Origin, version 19.0.

**Circular dichroism (CD) assay**

The purified protein was concentrated to 1 mg/ml in 20 mM Tris 8.0, 100 mM NaCl. Then, 1 mM $Zn^{2+}$ and $Mn^{2+}$ were added to 200 μg of protein incubated on ice for 1 h. Set the wavelength to 180-260 nm for scanning, observe the chromatographic peaks and use CDpro software for data analysis and processing. Finally, the changes

566 in the secondary structure of the protein are judged by comparing the ratio changes of
567 the indicators ($\alpha$-helixs, $\beta$-sheets, $\beta$-turns and random coils).

568 **Isothermal titration calorimetry (ITC) assay**

569 The ITC experiment was carried out using Auto-ITC (Malvern, United Kingdom)
570 instrument at a constant temperature of 25 °C. During setting up the program, the
571 volume of the first drop of small molecules is 0.4 μl, and the volume of the remaining
572 18 drops is 2 μl per drop. After the experiment, use MicroCal ORIGIN software to
573 process and analyze the data. When investigating the binding ability of OxDC and
574 oxalic acid, 10 mM oxalic acid (60 μl) was used to titrate 340 μM (200 μl) OxDC.
575 During investigating the binding mode of $Zn^{2+}$ and OxDC, firstly, the purified protein
576 was dialyzed into a buffer containing 100 mM NaCl, 20 mM Bis-Tris (pH 6.0) and 20
577 mM EDTA. After 2 h of dialysis, multiple dialysis methods were used to remove the
578 ions. The protein was dialyzed into 100 mM NaCl, 20 mM Bis-Tris 6.0 buffer to
579 facilitate the removal of EDTA. The control protein does not need to be pre-treated
580 with EDTA.

581 **Digestive stability of OxDC *in vitro***

582 To determine if the $Zn^{2+}$ and $Mn^{2+}$ affect the stability of OxDC enzyme, we
583 performed susceptibility to protease assays. The OxDC protein was adjusted at 1.0
584 mg/mL in Tris-HCl buffer (20 mM Tris-HCl, pH 7.0), then incubated with 1mM
585 EDTA and 1mM $Zn^{2+}$ or $Mn^{2+}$, at last incubated with 1mM Trypsin for 1, 5, 15 min at
586 25℃. The quality ratio of OxDC to Trypsin was 500. Finally, digestive stability of
587 OxDC was verified by 15% sodium dodecyl sulfate-polyacrylamide gel

588 electrophoresis (SDS-PAGE) and Colloidal Brilliant Coomassie Blue R-250 was used
589 to stain the gel.

590 **Statistical analyses**

591 All the grouped data were assessed by GraphPad Prism software 7.0 (GraphPad
592 Software, USA). Data were statistically calculated using t-test (two groups) or
593 one-way ANOVA. Independent experiments were performed at least five times with
594 similar results were considered significant if *P* values <0.05.

595 **Acknowledgments**

596 This work was supported in part by the Guangdong Key Laboratory for
597 Translational Cancer Research of Chinese Medicine (No. 2018B030322011),
598 Guangdong Province Universities and Colleges Pearl River Scholar Funded Scheme
599 (No. Caiyan Wang, 2019), Natural Science Foundation of Guangdong Province (No.
600 2017A030310501), and Scientific Research Project Funded by Traditional Chinese
601 Medicine Bureau of Guangdong Province (No. 20221170).

602 **Author contributions**

603 Caiyan Wang and Zhongqiu Liu conceived the project and designed the
604 experiments; Fang Wu, Yuanyuan Cheng, Peisen Ye, Xuehua Liu and Lin Zhang
605 carried out experiments and analyzed the data in this article; Yuanyuan Cheng, Fang
606 Wu, Jianfu Zhou and Rongwu Lin wrote the paper; Songtao Xiang and Caiyan Wang
607 advised and revised the manuscript. All authors approved the final version of the
608 manuscript, and all the authors declared no competing interests.

609 **Declaration of Competing Interest**

610 The authors have declared that no competing interest exists.

611

612

613

614

615

616

617

618

619

620

621

622

623

624

625

626

627

628

629

630

631

## References


1. Shoag J, Tasian GE, Goldfarb DS, Eisner BH. 2015. The New Epidemiology of Nephrolithiasis. Advances in Chronic Kidney Disease.
2. Pitrelli N, Basti M, Nardi M, Marrone A, Vacca M. 1995. [Giant bladder calculus. Report of a clinical case]. Minerva Chirurgica 50:155.
3. Liebman M, Costa G. 2000. EFFECTS OF CALCIUM AND MAGNESIUM ON URINARY OXALATE EXCRETION AFTER OXALATE LOADS. Journal of Urology 163:1565-1569.
4. Mandel NS, Mandel GS. 1989. Urinary tract stone disease in the United States veteran population. II. Geographical analysis of variations in composition. J Urol 142:1516-1521.
5. Zarembski PM, Hodgkinson A. 1969. Some factors influencing the urinary excretion of oxalic acid in man. Clinica Chimica Acta 25:1-10.
6. Robertson WG, Peacock M, Nordin BEC. 1968. Activity products in stone-forming and non-stone-forming urine. Clinical Science 34:579.
7. Marengo SR, Romani AM. 2008. Oxalate in renal stone disease: the terminal metabolite that just won't go away. Nat Clin Pract Nephrol 4:368-377.
8. Baumann JM, Casella R. 2019. Prevention of Calcium Nephrolithiasis: The Influence of Diuresis on Calcium Oxalate Crystallization in Urine. Advances in Preventive Medicine 2019:1-8.
9. Mager R, Neisius A. 2019. [Current concepts on the pathogenesis of urinary stones]. Urologe A 58:1272-1280.
10. Williams AW, Wilson DM. 1990. Dietary intake, absorption, metabolism, and excretion of oxalate. Seminars in Nephrology 10:2-8.
11. Mogna L, Pane M, Nicola S, Raiteri E. 2014. Screening of different probiotic strains for their in vitro ability to metabolise oxalates: any prospective use in humans? Journal of Clinical Gastroenterology 48 Suppl 1:S91-S95.
12. Turkmen K, Erdur FM. 2015. The relationship between colonization of Oxalobacter formigenes serum oxalic acid and endothelial dysfunction in hemodialysis patients: From impaired colon to impaired endothelium. Medical Hypotheses 84:273-275.
13. Anna, Zampini, Andrew, Nguyen, Emily, Rose, Manoj, Monga, Aaron. 2019. Defining Dysbiosis in Patients with Urolithiasis. Scientific Reports.
14. Ferraro PM, Curhan GC, Gambaro G, Taylor EN. 2019. Antibiotic Use and Risk of Incident Kidney Stones in Female Nurses. American Journal of Kidney Diseases 74:736-741.
15. Deng W, Yang L, Cai B. 2000. Long-term recurrence rate in the treatmnet of urethral stone with ESWL. BEIJING MEDICAL JOURNAL.
16. Khrmann KU, Rassweiler J, Alken P. 1993. The recurrence rate of stones following ESWL. World Journal of Urology 11:26-30.
17. Sanders ME, Guarner F, Guerrant R, Holt PR, Quigley EM, Sartor RB, Sherman PM, Mayer EA. 2013. An update on the use and investigation of probiotics in health and disease. Gut 62:787-796.
18. Parvez S, Malik KA, Kang SA, Kim HY. 2010. Probiotics and their fermented

food products are beneficial for health. Journal of Applied Microbiology 100:1171-1185.

19. Abratt VR, Reid SJ. 2010. Oxalate-degrading bacteria of the human gut as probiotics in the management of kidney stone disease. Advances in Applied Microbiology 72:63-87.

20. Giardina S, Scilironi C, Michelotti A, Samuele A, Borella F, Daglia M, Marzatico F. 2014. In Vitro Anti-Inflammatory Activity of Selected Oxalate-Degrading Probiotic Bacteria: Potential Applications in the Prevention and Treatment of Hyperoxaluria. Journal of Food Science 79:M384–M390.

21. Endo, Rin, Aoyagi, Hideki. 2018. Adsorption preference for divalent metal ions by Lactobacillus casei JCM1134. Applied Microbiology & Biotechnology.

22. Lin R, He J, Wu J, Cai X, Long H, Chen S, Liu H. 2017. Chemical modification of oxalate decarboxylase to improve adsorption capacity. International Journal of Biological Macromolecules 98:495-501.

23. Zhao C, Yang H, Zhu X, Li Y, Wang N, Han S, Xu H, Chen Z, Ye Z. 2017. Oxalate-Degrading Enzyme Recombined Lactic Acid Bacteria Strains Reduce Hyperoxaluria. Urology:S0090429517312414.

24. Campieri C, Campieri M, Bertuzzi V, Swennen E, Matteuzzi D, Stefoni S, Pirovano F, Centi C, Ulisse S, Famularo G. 2001. Reduction of oxaluria after an oral course of lactic acid bacteria at high concentration. Kidney International 60:1097-1105.

25. Ferraz R, Marques NC, Froeder L, Menon VB, Siliano PR, Baxmann AC, Heilberg IP. 2009. Effects of Lactobacillus casei and Bifidobacterium breve on urinary oxalate excretion in nephrolithiasis patients. Urological Research 37:95-100.

26. Ponnusamy, Sasikumar, Sivasamy, Gomathi, Kolandaswamy, Anbazhagan, Govindan, Sadasivam, Selvam. 2013. Secretion of biologically active heterologous oxalate decarboxylase (OxdC) in Lactobacillus plantarum WCFS1 using homologous signal peptides. BioMed research international 2013:280432-280432.

27. Sasikumar P, Gomathi… S. 2014. Recombinant Lactobacillus plantarum expressing and secreting heterologous oxalate decarboxylase prevents renal calcium oxalate stone deposition in experimental rats. Journal of Biomedical Science 21.

28. Roselli M, Finamore A, Britti MS, Konstantinov SR, Smidt H, Vos WD, Mengheri E. 2007. The novel porcine Lactobacillus sobrius strain protects intestinal cells from enterotoxigenic Escherichia coli K88 infection and prevents membrane barrier damage. Journal of Nutrition 137:2709-2716.

29. Anderson RC, Cookson AL, Mcnabb WC, Park Z, Mccann MJ, Kelly WJ, Roy NC. 2010. Lactobacillus plantarum MB452 enhances the function of the intestinal barrier by increasing the expression levels of genes involved in tight junction formation. BMC Microbiology 10.

30. Anukam KC, Reid G. 2007. Probiotics : 100 years ( 1907-2007 ) after Elie Metchnikoff ' s Observation Brief history of Elie Metchnikoff Probiotics beyond fermented dairy products.
31. Calesnick B, Dinan AM. 1988. Zinc deficiency and zinc toxicity. American Family Physician 37:267-70.
32. Beyersmann D. 2010. Homeostasis and Cellular Functions of Zinc. Materialwissenschaft Und Werkstofftechnik 33:-.
33. Tran CD, Ball JM, Sundar S, Coyle P, Howarth GS. 2007. The Role of Zinc and Metallothionein in the Dextran Sulfate Sodium-Induced Colitis Mouse Model. Digestive Diseases and Sciences 52:2113-2121.
34. Ren Z, Zhao Z, Wang Y, Huang K. 2011. Preparation of Selenium/Zinc-Enriched Probiotics and Their Effect on Blood Selenium and Zinc Concentrations, Antioxidant Capacities, and Intestinal Microflora in Canine. Biological Trace Element Research 141:170-183.
35. Mehta M, Goldfarb DS, Nazzal L. 2016. The role of the microbiome in kidney stone formation. International Journal of Surgery:607.
36. Yung-Ching C, Ahmad M, Jiang W, Khan SR, Gray JJ, Mckee M. 2018. Modulation of calcium oxalate dihydrate growth by phosphorylated osteopontin peptides. Journal of Structural Biology 204:S1047847718301680-.
37. Dunwell JM, Purvis A, Khuri S. 2004. Cupins: the most functionally diverse protein superfamily? Phytochemistry 65:7-17.
38. Anand R, Dorrestein PC, Kinsland C, Begley TP, Ealick SE. 2002. Structure of oxalate decarboxylase from Bacillus subtilis at 1.75 A resolution. Biochemistry 41:7659.
39. Burrell MR, Just VJ, Bowater L, Fairhurst SA, Requena L, Lawson DM, Bornemann S. 2007. Oxalate decarboxylase and oxalate oxidase activities can be interchanged with a specificity switch of up to 282,000 by mutating an active site lid. Biochemistry 46:12327-36.
40. Svedruzi D, Jónsson S, Toyota CG, Reinhardt LA, Richards N. 2005. The enzymes of oxalate metabolism: Unexpected structures and mechanisms. Archives of Biochemistry and Biophysics 433:176-192.
41. Kraut DA, And K, Herschlag D. 2003. Challenges in enzyme mechanism and energetics. Annual Review of Biochemistry 72:517-571.
42. Tanner A, Bowater L, Fairhurst SA, Bornemann S. 2001. Oxalate decarboxylase requires manganese and dioxygen for activity. Overexpression and characterization of Bacillus subtilis YvrK and YoaN. Journal of Biological Chemistry 276:43627.
43. Turgut M, Unal I, Berber A, Demir TA, Mutlu F, Aydar Y. 2008. The concentration of Zn, Mg and Mn in calcium oxalate monohydrate stones appears to interfere with their fragility in ESWL therapy. Urological Research 36:31-38.
44. Huang Y, Zhang YH, Chi ZP, Huang R, Cao SZ. 2019. The Handling of Oxalate in the Body and the Origin of Oxalate in Calcium Oxalate Stones. Urologia Internationalis 104:1-10.

764 45. Anonymous. 2014. Degradation of oxalic acid by the mycoparasite
765 Coniothyrium minitans plays an important role in interacting with Sclerotinia
766 sclerotiorum. Environmental Microbiology 16.
767 46. Khan SR. 2013. Animal Models of Calcium Oxalate Kidney Stone Formation.
768 Animal Models for the Study of Human Disease:483-498.
769 47. Emsley P, Lohkamp B, Scott WG, Cowtan K. 2010. Features and development
770 of Coot. Acta Crystallographica Section D: Biological Crystallography 66.
771

772

## Figure legends

**Figure 1. Clinical data analysis of the effects of Zinc Gluconate on the patients with CaOx stones.** (A) Four cohorts were devised in this study: the antibiotic treatment, the antibiotic combines with Zinc Gluconate, the patients with CaOx Kidney stones and the patients with non-kidney stones. The last two groups were not shown in the figure. (B) Bar plot analysis of several major intestinal microbiota in the human intestinal. (C) The analysis the abundance of several *Firmicutes* in four groups. (D) The analysis the species levels of bacterial composition in four groups.

**Figure 2. The protection of $Zn^{2+}$ on *Lactobacillus* and the therapeutic effect on rats with CaOx stones.** (A) The influence of seven common antibiotics on the growth of *L. casei*. (B) The influence of four common divalent metal ions ($Zn^{2+}$, $Mn^{2+}$, $Mg^{2+}$, $Ca^{2+}$) on the ability of lactobacilli to tolerate Amp. (C) The survival of *L. casei* under antibiotic stress after the addition of $Zn^{2+}$. (D) Effect of $Zn^{2+}$ on the tolerance of *L. casei* to oxalic acid. (E) Schematic diagram of the mechanism by which $Zn^{2+}$ protects *Lactobacillus* and promotes its proliferation. All assays were replicated more than three times. * indicates $P<0.05$; ** indicates $P<0.01$; *** indicates $P<0.001$.

**Figure 3. The effect of $Zn^{2+}$ on the inflammatory response and the degree of kidney damage in rats with CaOx stones.** (A)Results of hematoxylin-eosin staining of rat kidney tissue after 11 d of modeling. The control group was given the same volume of 0.9% saline. The red arrow shows the sites of stone growth. (B) Diagram of the relationship between inflammatory factors, osteopontin and CaOx stones. (C) Changes of urea nitrogen in serum and urine in rats with CaOx stones. (D) Changes in mRNA levels of osteopontin and its receptor (CD44) in kidney tissue. (E) The expression level of inflammatory factors (TNFα , IL-1β) in the kidney tissue of rats with CaOx stones were detected by qRT-PCR. The black * means compared with the

798 control group, and the red * means with Amp+Stone as the reference group. *
799 indicates $P<0.05$; ** indicates $P<0.01$; *** indicates $P<0.001$.

800 **Figure 4. Association of oxalate-degrading bacteria and OxDC with CaOx stone**
801 **formation in kidney stones patients and the crystal structure of *L. farciminis***
802 **OxDC**. (A) The mRNA level of OxDC in the non- kidney stones and CaOx kidney
803 stones patients. The number of patients in the non-kidney stones group and CaOx
804 kidney stones group is 25 and 27, respectively. Measurement data were represented as
805 the mean ± SEM. Unpaired t-test was conducted to assess data with a normal
806 distribution and equal variance. (B) Chromatogram from size-exclusion
807 chromatography analysis. The black line represents the chromatogram of three
808 standard molecular weight proteins (440, 158, and 75 kDa), and the OxDC
809 chromatogram is indicated with the red line. (C) Domain distribution and structure of
810 a single subunit of OxDC. The N-terminal and C-terminal cupin domains are colored
811 gray and orange, respectively. $Mn^{2+}$ is presented as pink spheres. (D) OxDC's
812 topology diagram. The shaded color indication is consistent with Figure A. The
813 columnar is represented as α-helix, and the arrow stands for β-sheet. (E) The
814 structural similarity of the two functional domains. The N-terminal and C-terminal
815 cupin domains are colored gray and orange, respectively. The software Pymol was
816 used for structural Alignment. (F) The hexamer structure of OxDC in cartoon mode
817 (front view and view after rotating 90° along the Y-axis). * indicates $P<0.05$; **
818 indicates $P<0.01$; *** indicates $P<0.001$.

819 **Figure 5. Discovery and verification of key residues in the active pocket.** (A)
820 Multiple amino acid sequence alignments between OxDC proteins from different
821 species, including key fragments of two domains (red indicates highly conserved
822 residues, asterisks indicate the five selected mutation sites). The GenBank identifiers

(GI) for these species are 908212467 (*L. farciminis*) and 760455501 (*B. subtilis*), 1437302606 (*S. nepalensis*), 814506590 (*S. pneumoniae*), 1330860547 (*E. cancerogenus*), 126221798 (*B. pseudomallei*), respectively. (B) Schematic diagram showing coordination between key residues in N-cupin domains and $Mn^{2+}$. FMT stands for formic acid. (C) Coordination between key residues in C-cupin domains and $Mn^{2+}$. FMT is shown as a ball-and-stick model. (D) The enzyme activity of mutants and WT are verified *in vitro*. (E) Photographs taken under a fluorescence microscope after the transfection of exogenous plasmid (pEGFP, WT-pEGFP, E162D-pEGFP, E333D-pEGFP) into HEK293 cells. (F) Expression of apoptosis and inflammatory factors (Caspase3, IL-1β, and TNFα) in HEK293 cells. * indicates $P<0.05$; ** indicates $P<0.01$; *** indicates $P<0.001$.

**Figure 6**. **Discovered and verified the special effect of $Zn^{2+}$ on OxDC.** (A) Effects of common divalent metal ions on OxDC enzyme activity. The highest activity was set as 100% as a reference, the control group is the group without metal ion treatment and assays were carried out using a methylene blue-potassium dichromate system. (B) The effect of $Zn^{2+}$ and $Mn^{2+}$ on the secondary structure of OxDC tested by CD. (C) The influence of $Zn^{2+}$ on OxDC's thermal stability. (D) Schematic diagram of the binding pocket of $Zn^{2+}$ competitively binding to $Mn^{2+}$ (E) The binding ability of OxDC with $Zn^{2+}$ under different treatment conditions was determined by ITC experiments. For processing of data from the protein activity experiment, * indicates $P<0.05$.

**Figure 7. The effect of metal ion on the digestive stability of OxDC.** (**A**) Chromatogram from size-exclusion chromatography analysis. (**B**) OxDC protein thermal shift assay. (**C**) *In vitro* digestive stability of OxDC with trypsin. (**D**) The sketch map which the important of metal ions $Zn^{2+}$ and $Mn^{2+}$ for OxDC.

**Table 1. Data collection and refinement statistics**

| | |
|---|---|
| Data collection | |
| Space group | P21 |
| a, b, c (Å) | 92.96, 122.84, 115.22 |
| α, β, γ (°) | 90.00, 92.47, 90.00 |
| Resolution (Å) | 48.00-2.79 (2.84-2.79)[a] |
| $CC_{1/2}$ | 0.944 (0.810) |
| $R_{merge}$[b] | 0.141 (0.751) |
| I/σ(I) | 19.89 (1.94) |
| Completeness (%) | 96.94 (97.01) |
| Redundancy | 6.3 (6.0) |
| Refinement | |
| Resolution (Å) | 48.00-2.79 (2.79-2.84) |
| No. reflections | 62185 (1795) |
| $R_{work}$[c] /$R_{free}$[d] | 0.197/0.229 |
| No. atoms | |
| Protein | 16035 |
| Ligand | 18 (FMT),12 (MN) |
| Water | 248 |
| B-factors (Å$^2$) | |
| Protein | 35.8 |
| Ligand | 32.6 (FMT),36.5 (MN) |
| Water | 40.8 |
| R.m.s deviations | |
| Bond lengths (Å) | 0.007 |
| Bond angles (°) | 1.109 |
| Ramachandran favored (%) | 97.37 |
| Allowed | 2.33 |
| Outliers (%) | 0.30 |

[a]Values in parentheses are for the highest-resolution shell. [b]$R_{merge} = \Sigma |(I - < I >)|/\sigma(I)$, where I is the observed intensity. [c]$R_{work} = \Sigma_{hkl} ||Fo| - |Fc||/ \Sigma_{hkl} |Fo|$, calculated from working data set. [d]$R_{free}$ is calculated from 5.0% of data randomly chosen and not included in refinement.

855 **Figure 1:**

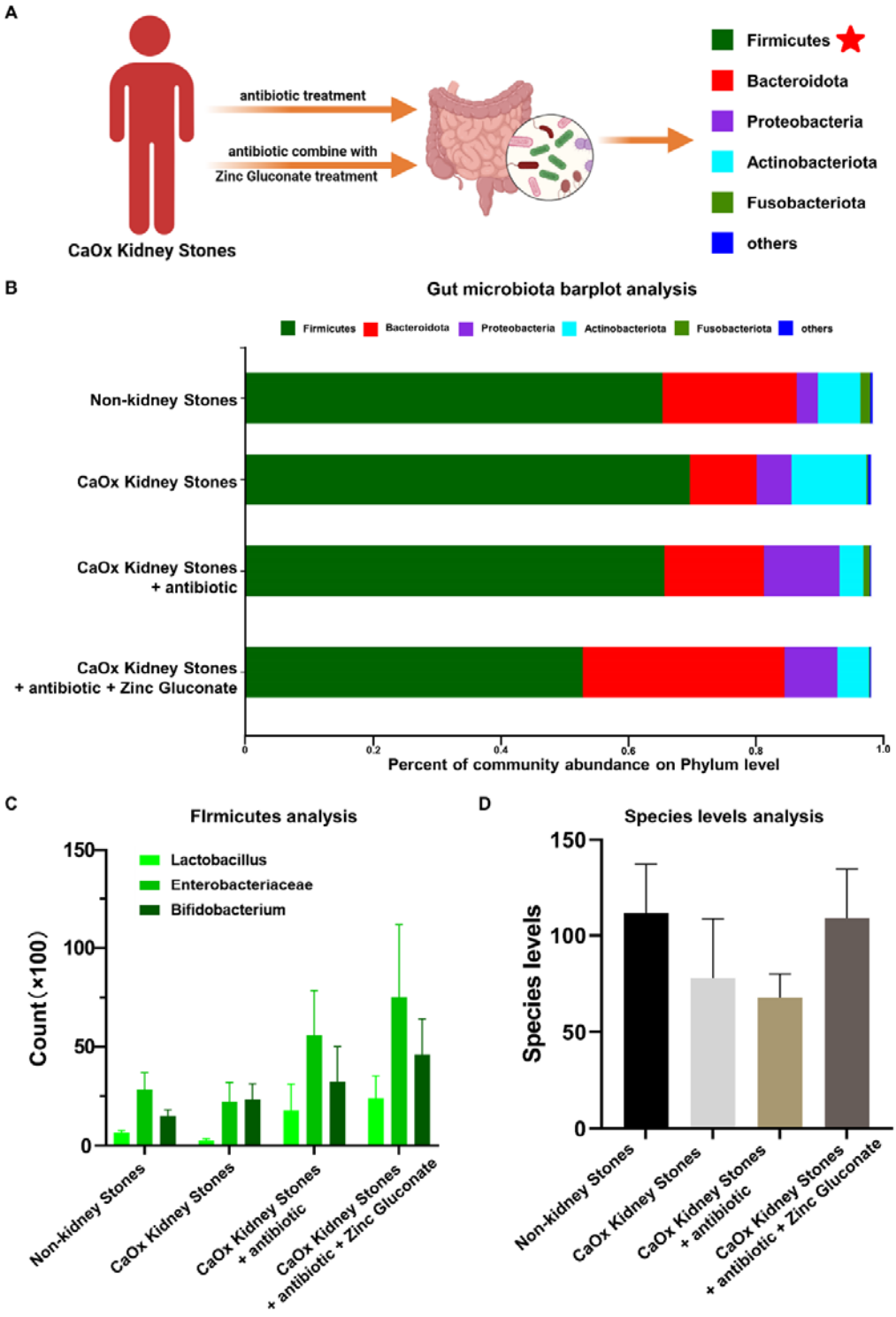


856

857

858 **Figure 2：**

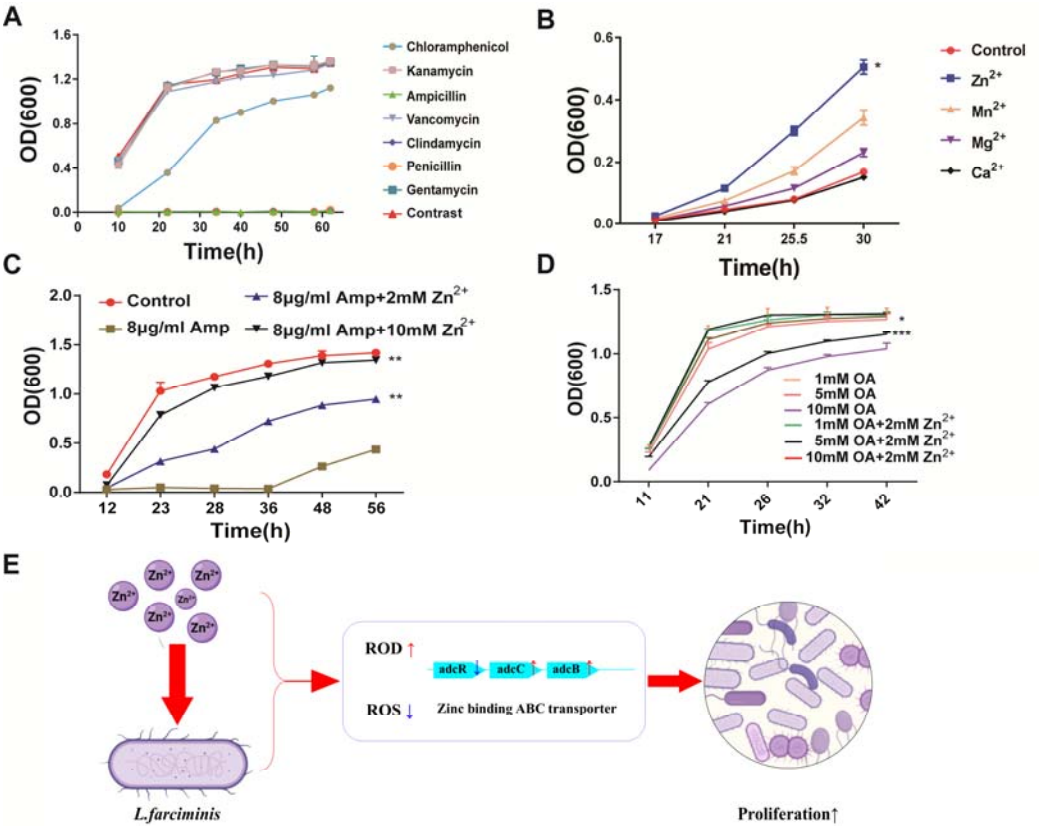


859

860

861 **Figure 3：**

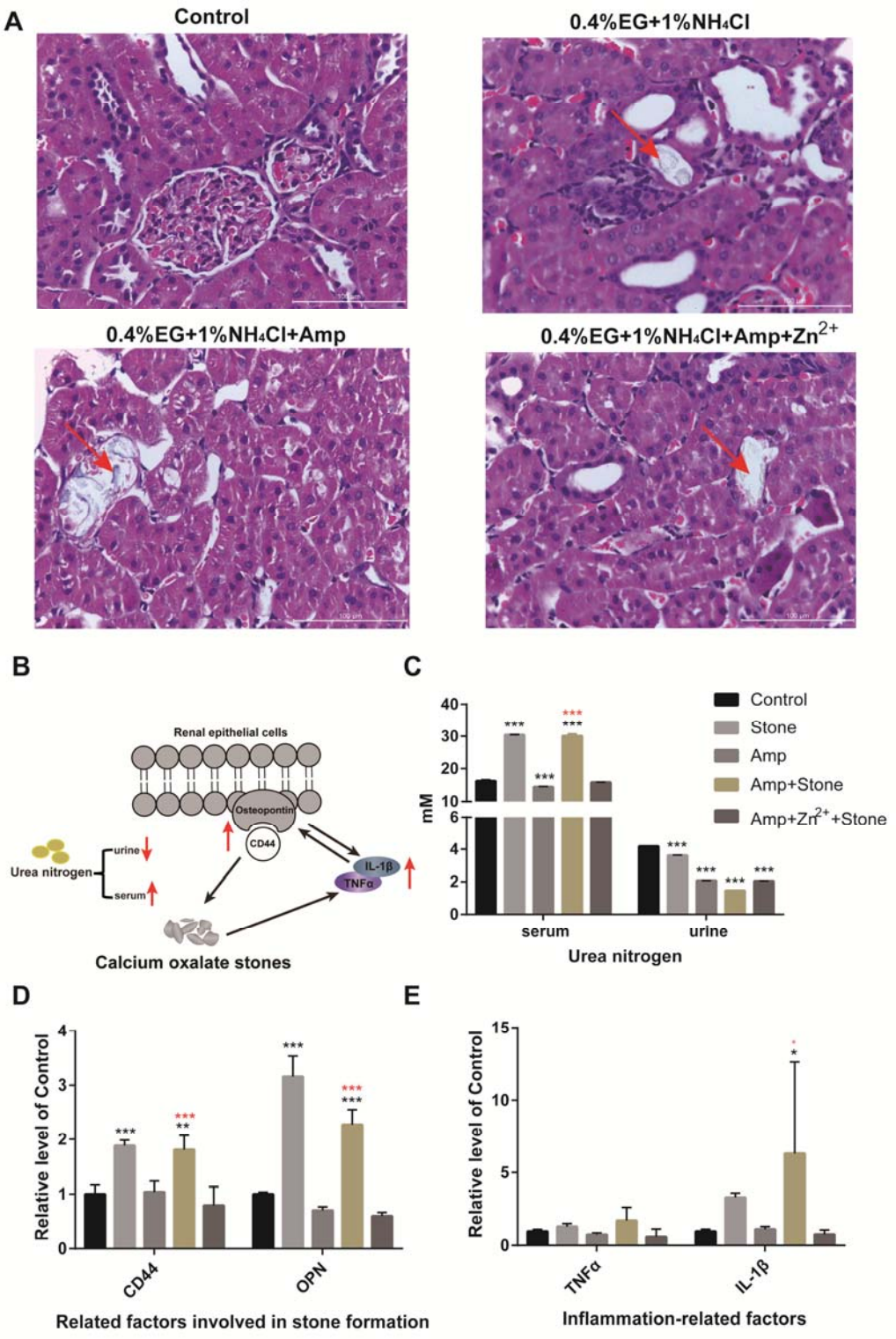


862

863

**Figure 4：**

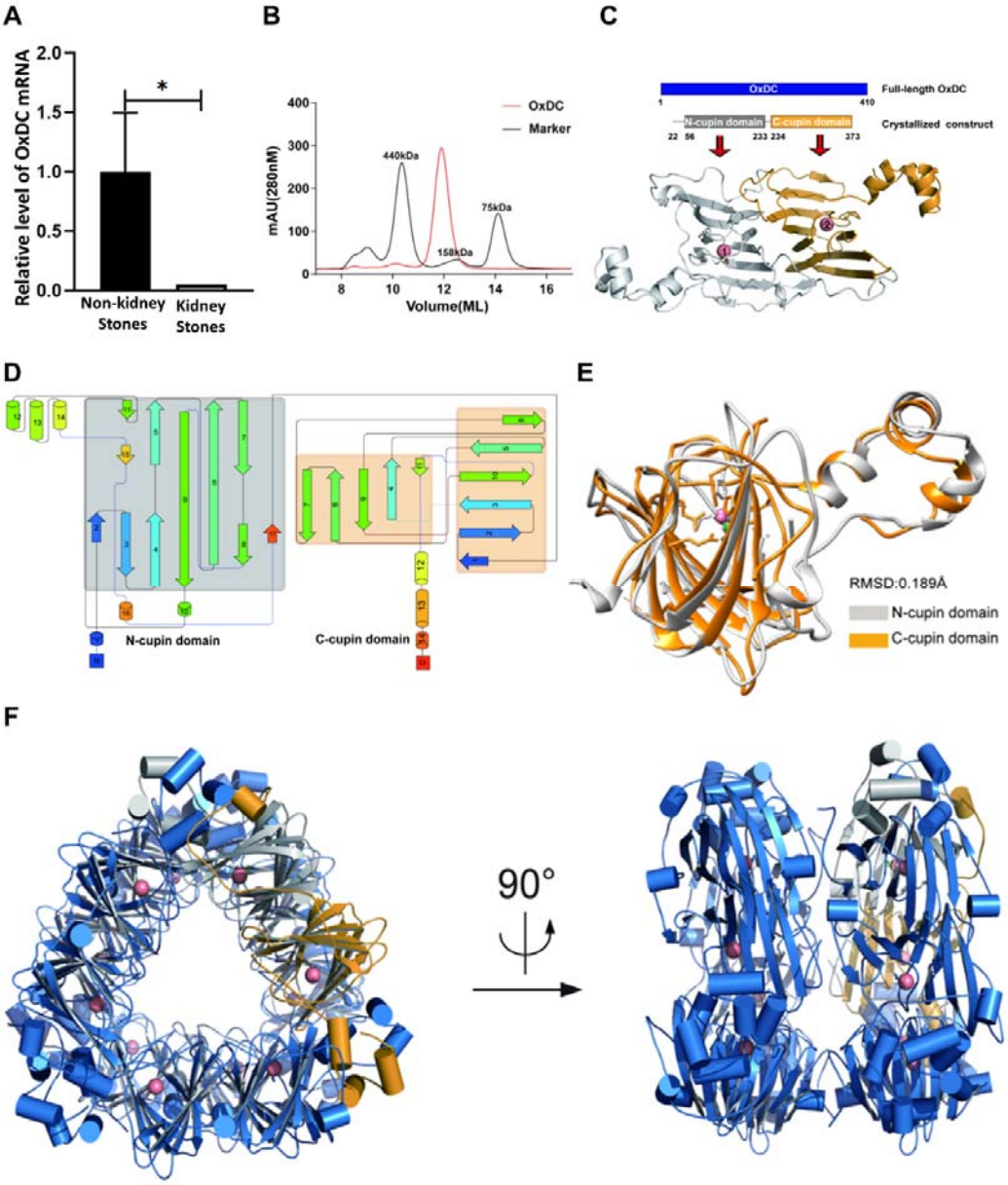


865

866

867 **Figure 5 :**

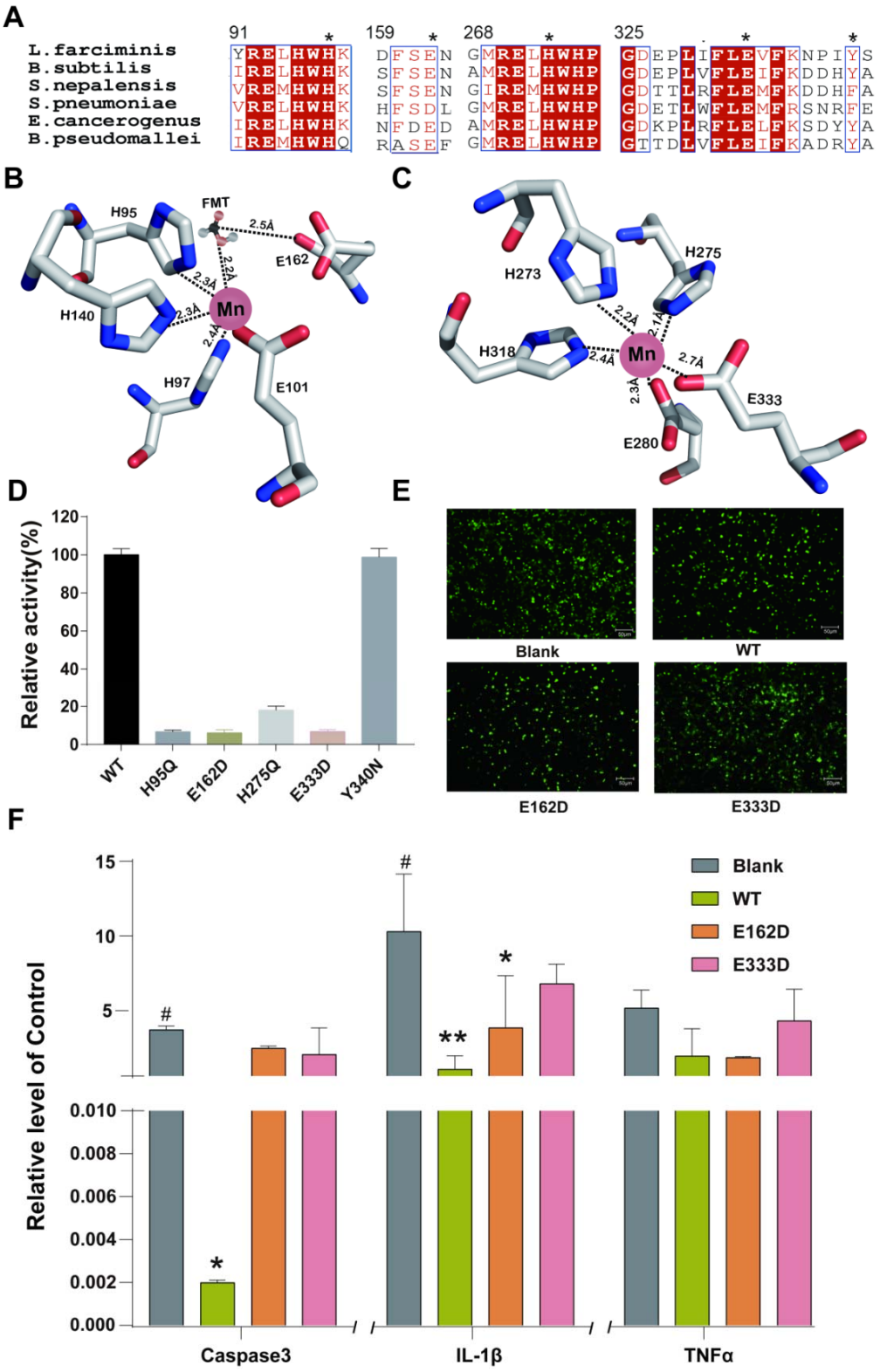


868

869

870 **Figure 6：**

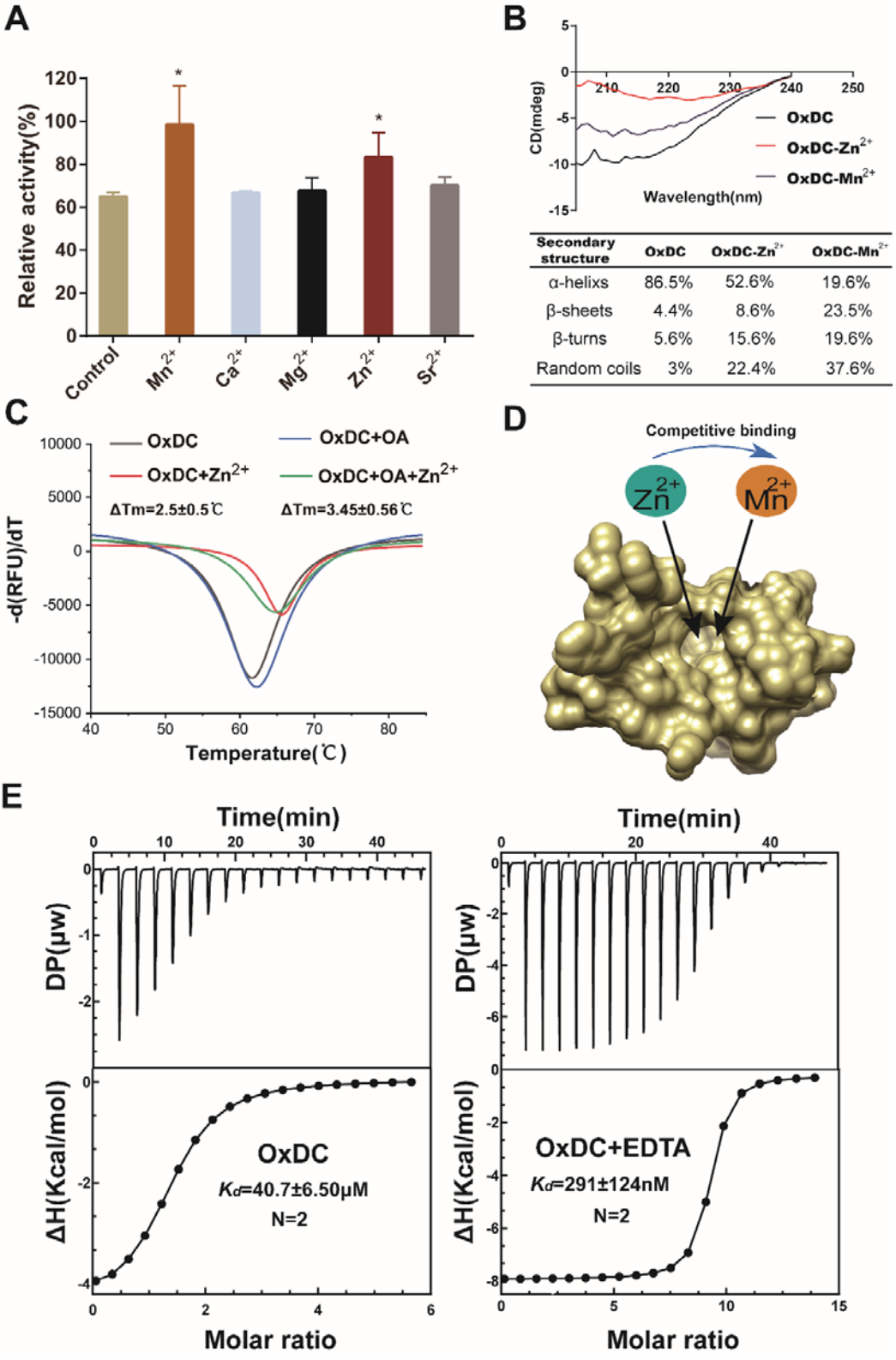


| Secondary structure | OxDC | OxDC-$Zn^{2+}$ | OxDC-$Mn^{2+}$ |
|---|---|---|---|
| α-helixs | 86.5% | 52.6% | 19.6% |
| β-sheets | 4.4% | 8.6% | 23.5% |
| β-turns | 5.6% | 15.6% | 19.6% |
| Random coils | 3% | 22.4% | 37.6% |

871

872

873 **Figure 7：**

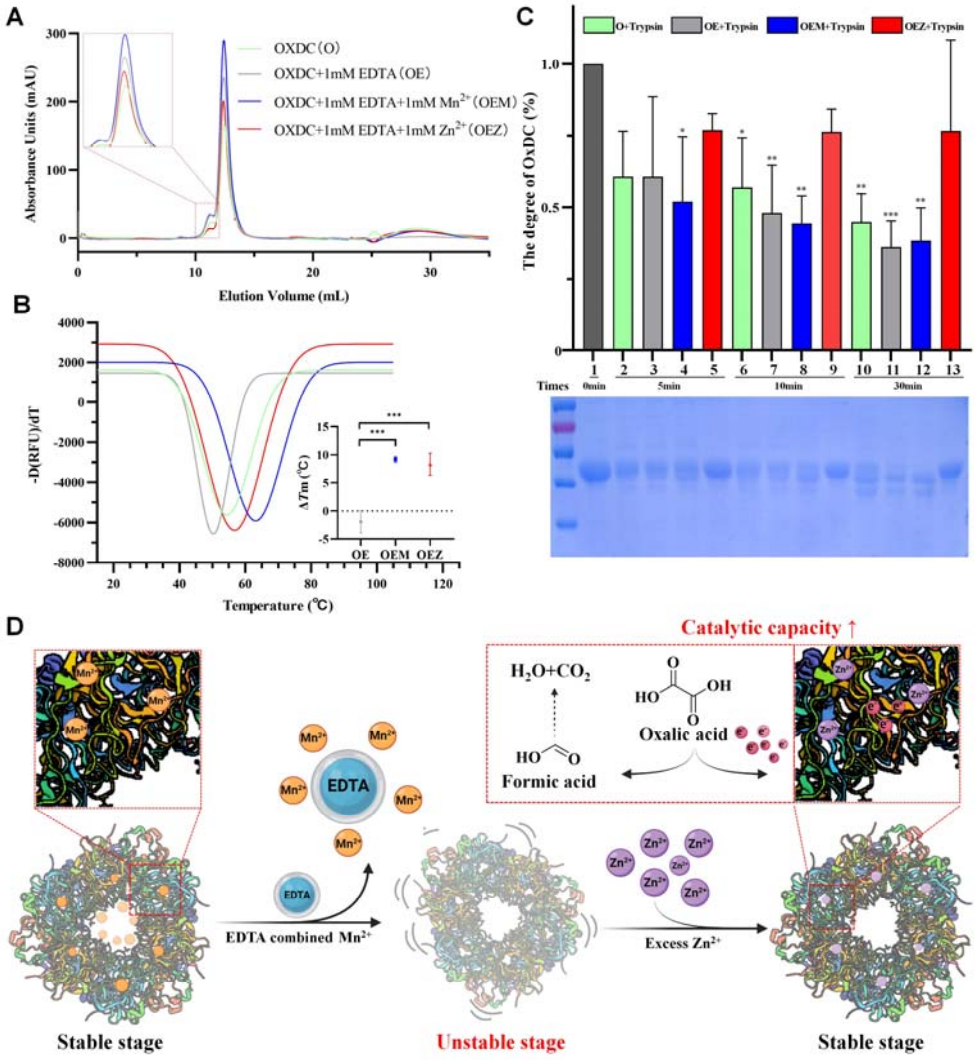


874

875

876

877

878

879

880

881

882